Submicron-scale patterns on ferromagnetic–antiferromagnetic Fe/NiO layers by focused ion beam (FIB) milling

G.C. Gazzadi [a,*], P. Luches [a], S.F. Contri [b], A. di Bona [a], S. Valeri [b]

[a] *National Research Center, INFM-S3, Via G. Campi 213/a, 41100 Modena, Italy*
[b] *INFM-S3 and Dipartimento di Fisica Università di Modena e Reggio Emilia, Via G. Campi 213/a, 41100 Modena, Italy*

Abstract

With the aim of studying the magnetic properties of reduced-dimensionality magnetic systems we have patterned 250 nm- and 500 nm-size square elements on Fe/NiO layers by 30 keV Ga^+ focused ion beam (FIB) milling, varying beam current and pixel dwell time. By high resolution scanning electron microscope (SEM) imaging and atomic force microscopy (AFM) analysis we found that island size decreases from the nominal value by increasing the beam current and features sharpness improves on increasing the dwell time. The top surface of the isolated features has a pronounced edge bending which may be as high as 9 nm with respect to the flat inner area of the island and decreases as dwell time grows. By varying the ion fluence we found that such a shape is related to a surface swelling effect occurring at low ion fluence in the irradiated areas. The swelling-related damage at the edges is expected to influence the magnetic properties of the patterned features.
© 2004 Elsevier B.V. All rights reserved.

1. Introduction

Magnetic properties of ferromagnetic (FM)/antiferromagnetic (aFM) multilayers are a subject of considerable interest owing to their peculiar properties, such as exchange bias, which can be exploited in many possible applications including non-volatile magnetic random access memories. In this context the Fe/NiO system is a suitable prototype to study the magnetic behaviour of a FM/aFM interface both for the large NiO Nèel temperature (523 K) and because of the small lattice mismatch allowing epitaxial growth of Fe film on

---

* Corresponding author. Tel.: +39 59 2055323; fax: +39 59 374794.
E-mail address: gazzadi@unimo.it (G.C. Gazzadi).

NiO surface [1,2]. Lateral confinement of these systems in dimensions of the order of tens or hundreds of nanometers, is performed in order to study the changes of magnetic properties with size, spacing and shape of the isolated structures. Since the spin configuration of each structure is strongly dependent on its crystal structure and on the defects it presents, particularly at the edges, we focus here on a detailed study of these aspects.

Many of the techniques employed for submicron scale patterning of magnetic media are lithographic and involve resist process with etching and cleaning steps. On the contrary, ion beam milling techniques [3,4] offer high resolution patterning in a single step directly on the sample, which can then be magnetically characterized without any further processing. Focused ion beam (FIB) milling has been proved to be effective in isolating single magnetic units either by inducing localized damage [5] or by direct removal of parts of a thin film [3,4]. With the latter approach we have recently patterned Fe thin films obtaining interesting magnetic properties dependence on the pattern structure [6].

In this work we report on submicron patterning of Fe/NiO layers epitaxially grown in the (001) orientation on MgO(001) substrates and capped with an MgO layer. Arrays of 500 nm and 250 nm square elements with spacing/size ratio of two were patterned in a FIB-scanning electron microscope (SEM) Dual Beam system by 30 keV Ga ion beam erosion of the thin films. Parameters like beam spot size, and pixel dwell time, playing an important role in determining the final shape of the isolated features [7,8], were systematically varied. The surface morphology and overall shape of the features were studied by in situ high-resolution SEM imaging and by ex situ atomic force microscopy (AFM) imaging.

2. Experimental

MgO(001) single crystal substrate was chosen since its lattice parameter ($a_{MgO} = 4.212$ Å) is suitable for epitaxial growth of NiO ($a_{NiO} = 4.176$ Å). Ni and Fe were evaporated in a UHV MBE system (base pressure lower than 5×10^{-11} Torr) from

Knudsen cells, on ex situ cleaved substrates. Deposition rates were calibrated by a quartz crystal microbalance. 10 nm NiO films were grown at a rate of 0.5 ML/min, keeping the MgO substrate at 520 K and depositing Ni in a background oxygen pressure of 1×10^{-7} Torr. 10 nm Fe films were subsequently grown at RT on top of the NiO film with the same deposition rate for NiO. Finally the samples were capped with 10 nm MgO films to protect the Fe film surface with a transparent material, suitable for magneto-optical characterization. Chemical analysis of the grown layers was performed by X-ray photoelectron spectroscopy (XPS) and their crystalline quality was followed step by step through secondary electron imaging (SEI) [9] with a primary electron beam of 1 keV.

FIB patterning was performed in a Dual Beam system FEI DB235M, combining a Ga$^+$ FIB and a thermal field emission SEM, working at coincidence on the sample. Nominal resolutions of the two columns are 7 nm at 30 keV for FIB and 2 nm over a wide energy range for SEM. Patterns were generated from black and white bitmap files, containing 8×8 array of square islands with a pitch/size ratio of two. FIB was rastered from top-left to bottom-right of the pattern along the x (horizontal) direction. The beam was switched on for black pixels and blanked for white. Three different apertures were chosen corresponding to nominal current values of 50, 100 and 300 pA, and nominal beam sizes of 15, 20 and 25 nm, respectively. Actual measured currents were 60, 144 and 398 pA, respectively. For each current, increasing dwell times (DT) of 1, 10 and 100 μs were employed, corresponding to decreasing rastering repetition numbers, in order to maintain the ion fluence constant. AFM characterization of the patterned samples was perfomed in air, working in contact mode with conventional pyramidal-shape cantilevers.

3. Results and discussion

From the comparison between the MgO(001) and the NiO film SEI patterns, shown in Fig. 1(a) and (b) it is evident that NiO exhibits the
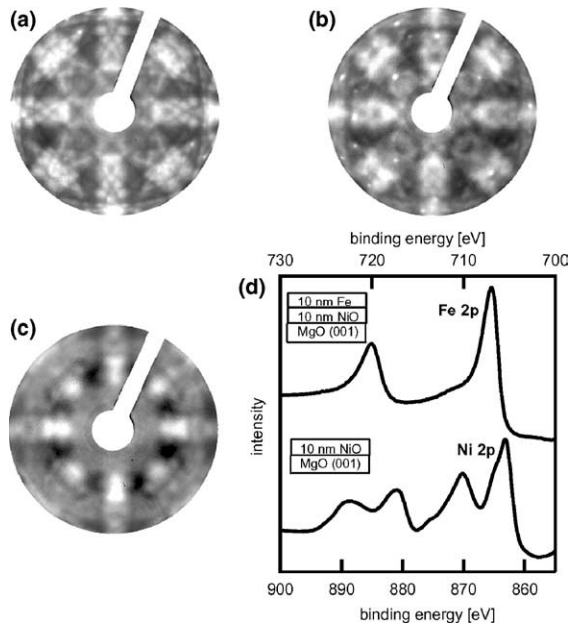
Fig. 1. SEI images of MgO(001) substrate (a), 10 nm NiO film on MgO(001) (b), 10 nm Fe film on 10 nm NiO/MgO(001) (c) and Ni2p and Fe2p XPS spectra for the 10 nm NiO film and for 10 nm Fe film (d).

face centred cubic rock-salt crystalline structure as MgO, with the NiO(001)‖MgO(001) and NiO[100]‖MgO[100] epitaxial relationship. The small lattice mismatch (3.1%) between body centred cubic Fe(001) and NiO(001) allows Fe epitaxial growth on NiO(001) surface with the Fe(001)‖NiO(001) and Fe[100]‖NiO[110] orientation, as shown in the SEI pattern in Fig. 1(c). Fig. 1(d) displays the Ni 2p XPS spectrum of 10 nm NiO film, exhibiting the characteristic bulk-like lineshape. The Fe 2p lineshape is consistent with a bulk-like non-oxidized Fe film.

The samples were milled to a depth of 40 nm with an ion fluence of 2.3×10^{17} ions/cm^2, in order to completely remove the MgO/Fe/NiO tri-layer. Depth versus ion fluence calibration was performed in situ by high resolution SEM imaging of the sample under tilted view, so that the depth component could be resolved. Subsequent AFM analysis confirmed the measured depths within ±5 nm. We also checked by X-ray microanalysis the composition of a milled region, in between

two islands. The absence of Ni and Fe signals and the appearance of Ga along with Mg and O lines confirmed that the tri-layer had been completely removed.

In Fig. 2, top view SEM micrographs of the patterns milled with increasing FIB current and DT = 1 μs are shown. For I = 60 pA the DT = 100 μs pattern is also reported. In the inset (e) a summary of the islands size as measured by the SEM images is displayed. Each SEM image shows a porous texture where the material has been removed by FIB milling and islands consisting of untouched sample areas. All features are characterized by a square shape with decreasing size and increasing roundness as the beam current grows. Within each island three distinct brightness region can be identified on moving from the outer edge to the center: a very bright and thin edge, a darker thick region beside and a brighter area at the center. This behaviour, as AFM analysis will
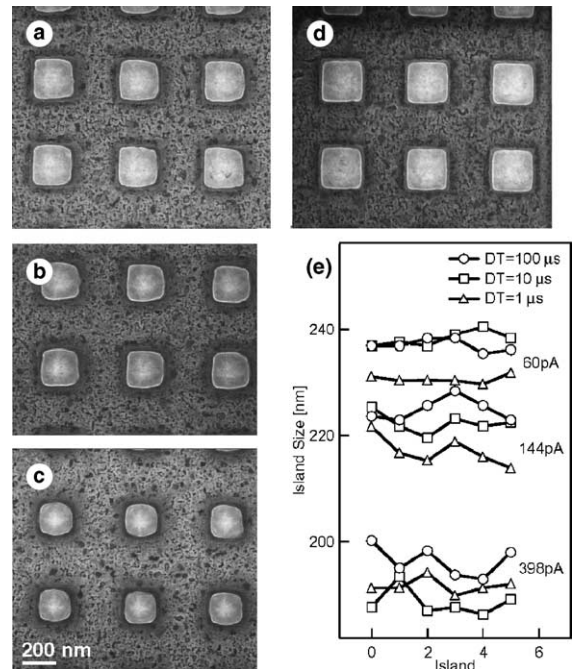
Fig. 2. Top view SEM micrographs of FIB patterns milled with I = 60 pA (a), I = 144 pA (b), I = 398 pA (c), DT = 1 μs and I = 60 pA, DT = 100 μs (d) and islands size for all milling conditions as measured from SEM images (e).

clarify, reflects the height profile of the top island surface, which shows an elevated rim at the edge, declining to a lower flat region in the middle.

Curves values reported in Fig. 2(e) correspond to the square root of the islands area. The visual trend observed for the images is confirmed: the average island size decreases with beam current, being 235, 225 and 192 nm for $I = 60$, 144 and 398 pA, respectively. This can be explained by the increasing beam spot size, with consequent longer beam tails which contribute more significantly to erosion at the border of the milling pattern, i.e at the islands edges. Within each current value another trend versus DT is apparent. Features size increases with DT, being minimum for DT = 1 μs. This behaviour is also linked to a better definition of the islands shape, which are more squared and have straighter sides, as the visual comparison between the two images for I = 60 pA and DT = 1 and 100 μs confirms. In this case we consider the repetitions number, which is inversely proportional to DT, as a major responsible. The more the beam passes around a feature the higher is the probability that factors like sample drifts or milling upon beam blanking may affect the shape resolution. Concerning the lack of DT dependence at 398 pA, we believe that the large beam spot size at this high current becomes dominant in defining the island shape over the aforementioned effects.

In Fig. 3, AFM 3 d images and the related line profiles for the conditions corresponding to Fig. 2(a)–(c) are shown. The most characteristic feature common to all islands is the concave surface. The surface contour is strongly bended-up at the four square vertices and gradually declines, symmetrically, toward the island center where a flat region, at the height level of the original surface, is present. Line profiles taken along the FIB milling direction, shown in Fig. 3(d), confirm that island width decreases with current and the flat region between edge tips progressively reduces, disappearing in the highest current curve. From these line profiles we have quantified the edge bending. In Fig. 3(e) the average height of the edge maxima with respect to the center of the island is plotted. As a general trend, the curves show a marked dependence on
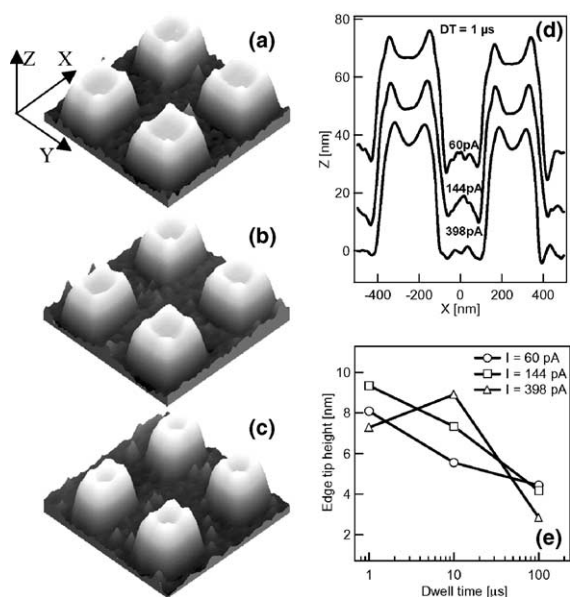
Fig. 3. AFM 3d images of the FIB patterns for $I = 60$ pA (a), $I = 144$ pA (b), $I = 398$ pA (c), DT = 1 μs, and the corresponding line profiles (d) shifted along Z to allow the comparison and edge tip height versus DT for the three ion beam current employed (e).

DT, with values monotonically decreasing as DT increases. Values as high as 9 nm are halved on passing from DT = 1 to DT = 100 μs. On the contrary, the dependence versus beam current at fixed DT is less pronounced, but indicates that absolute values increase on passing from 60 to 144 pA. Concerning the island walls, the step profile is similar for all milling conditions and shows three slope regions on going from the island base to the top. A first region with the steeper slope (45°) extends up to 70% of the step height, then slope suddenly decreases to 14° within a very short height interval, creating a visible edge in the wall profile and finally increases again to 18° in the top, bended region. The height of this final region is around 10–15 nm, a value consistent with MgO capping layer thickness. Therefore, the edge along the wall profile might be caused by a differential sputtering yield between MgO and Fe in the layer below. However, this point and the walls profile analysis has to be studied in more detail because step profile measurements are very critical with conventional AFM probes.

To investigate the origin of edge bending we have milled patterns of 500 nm square islands, 1 μm pitch, with decreasing ion fluence and analyzed the height profiles by AFM. The reason for reducing the ion fluence is that on several crystalline materials like Si, Ge, SiC a surface swelling effect has been reported for those areas irradiated by a low fluence, before sputtering erosion took place [10,11]. The effect is mainly explained by ion-induced amorphization of the crystalline structure, causing a local decrease of the material density and consequent volume expansion at the surface, although Ga ions implantation may also have a role. We set irradiation conditions of $I = 150$ pA, DT = 1 μs and ion fluences of 2.3×10^{17}, 6.9×10^{16} and 2.3×10^{16} ions/cm^2. In Fig. 4 the AFM 3d images and the line profiles of the resulting patterns are shown. The pattern at the lowest fluence (Fig. 4(a)) already shows the surface swelling effect in the regions irradiated by FIB, while the square islands, untouched by the beam, remain at a lower height level characteristic of the original surface. The height difference between the two regions, as measured from the line profiles, is around 3 nm. Increasing the ion fluence by a factor of three results in an enhancement of the swelling effect (Fig. 4(b)). The irradiated areas are now strongly protruding with respect to the untouched regions and the height difference rises to 5 nm. Irradiation at the highest fluence (Fig. 4(c)) pro-

duces the expected surface erosion with square islands having the surface edge bending, as observed in the previous patterns. The edge shape and height, measured with respect to the island center, exactly recall those obtained with the same milling conditions on the 250 nm islands of Fig. 3. From the evolution of the line profiles versus ion fluence in the region around the island edge we can ascribe the edge bending effect to swelling. In particular, it is clear that edge bending represents the tails of swelled areas. The profiles height at the island edge increases (1.8, 2.8 and 9.4 nm) and the tail progressively extends into the island as fluence grows. Being at an edge of the pattern, this evolution is related to the ion fluence deposited by the beam tails. The deposited ion fluence grows with time according to the beam current profile which is nominally gaussian. Therefore, the further the beam tail is from the center of the distribution the longer is the time required to reach the critical amorphization fluence, inducing the swelling effect. Within this picture we can now argue some hypotheses on the edge bending dependence versus beam parameters observed in Fig. 3(e). Edge bending increment for growing beam current can be related to the deeper amorphous layers produced by increasing the fluence rate, as reported for Si in literature [12]. The most evident dependence of edge bending versus DT it is difficult to explain. Data show that longer beam pulses produce lower swelling effects. We suggest that longer beam exposures may induce thermal spikes in the collisional cascade process [13] which help in annealing the amorphization damage and consequently reduce the swelling effect.

The amorphization and, possibly, the intermixing, associated to the swelling phenomenon, are expected to reduce the interface sharpness of the FM/aFM bilayer over a considerable portion of the nanomagnet area. The exchange bias effect is larger in presence of a sharp FM/aFM interface [14], therefore this partial interfacial broadening is in turn expected to reduce the exchange effect. In addition, the localization of damage at the edges of the nanostructures possibly decreases the configurational contribution [6,15] to the overall anisotropy of the magnetic structure.
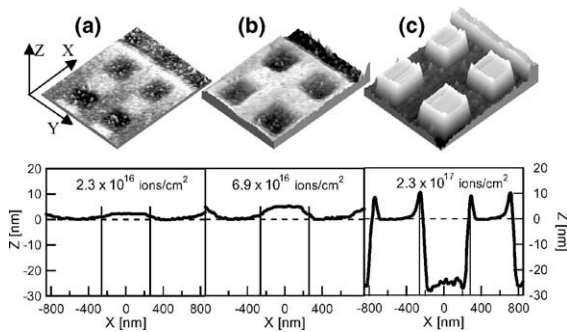
Fig. 4. AFM 3d images and corresponding line profiles for FIB patterns irradiated with increasing ion fluence, $I = 150$ pA, DT = 1 μs: 2.3×10^{16} ions/cm^2 (a), 6.9×10^{16} ions/cm^2 (b) and 2.3×10^{17} ions/cm^2 (c).

4. Conclusions

We have patterned 250 nm- and 500 nm-size square elements on Fe/NiO layers by 30 keV Ga^+ FIB erosion of a $MgO_{10nm}/Fe_{10nm}/NiO_{10nm}/MgO_{bulk}$ sample, varying the beam current (60, 144 and 398 pA) and the pixel dwell time (1, 10, 100 μs). By SEM and AFM analysis we found that island size decreases from the nominal value by increasing the beam current and sharpness of the features is improved on increasing the dwell time. The top surface of the isolated elements has a characteristic curved-shape, with a pronounced edge bending which may be as high as 9 nm with respect to the flat inner area of the island and decreases as dwell time grows. By varying the ion fluence we found the origin of this shape, which is related to a surface swelling effect occurring at low ion fluence in the irradiated areas. These findings, in particular the swelling-related damage at the edges, are expected to have a strong influence on the FM/aFM exchange bias and the configurational anisotropy of the patterned features.

Acknowledgements

References

[1] R. de Masi, D. Reinicke, F. Müller, P. Steiner, S. Hüfner, Surf. Sci. 515 (2002) 523.

[2] P. Luches, M. Liberati, S. Valeri, Surf. Sci. 532–535 (2003) 409.

[3] B.D. Terris, L. Folks, D. Weller, J.E.E. Baglin, A.J. Kellock, H. Rothuizen, P. Vettiger, Appl. Phys. Lett. 75 (1999) 403.

[4] G. Xiong, D.A. Allwood, M.D. Cooke, R.P. Cowburn, Appl. Phys. Lett. 79 (2001) 3461.

[5] C. Vieu, J. Gierak, H. Launois, T. Aign, P. Meyer, J.P. Jamet, J. Ferre', C. Chappert, V. Mathet, H. Bernas, Microelectron. Eng. 53 (2000) 191.

[6] P. Vavassori, D. Bisero, F. Carace, M. Liberati, A. di Bona, G.C. Gazzadi, S. Valeri, J. Magn. Mag. Mater., in press.

[7] H. Yamaguchi, A. Shimaze, S. Haraichi, T. Miyauchi, J. Vac. Sci. Tech. B 3 (1985) 71.

[8] F. Yongqi, N. Kok Ann Bryan, N.P. Hung, O.N. Shing, Rev. Sci. Instr. 71 (2000) 1006.

[9] M. Erbudak, M. Hochstrasser, E. Wetli, M. Zurkirch, Surf. Rev. Lett. 4 (1997) 179.

[10] C. Lehrer, L. Frey, S. Petersen, H. Ryssel, J. Vac. Sci. Technol. B 19 (2001) 2533.

[11] A. Lugstein, B. Basnar, G. Hobler, E. Bertagnolli, J. Appl. Phys. 92 (2002) 4037.

[12] S. Prussin, P.F. Zhang, Ion implantation technology, in: Proc. 11th Int. Conf. Ion Implantation Technology, IEEE, New York, 1997, p. 555.

[13] P. Sigmund, in: R. Behrisch (Ed.), Sputtering by Particle Bombardment I, Springer-Verlag, 1981.

[14] J. Nogués, T.J. Moran, D. Lederman, Ivan K. Schuller, K.V. Rao, Phys. Rev. B 59 (1999) 6984.

[15] R.P. Cowburn, A.O. Adeyeye, M.E. Welland, Phys. Rev. Lett. 81 (1998) 5414.